Journal of ELECTRONIC MATERIALS, Vol. 42, No. 6, 2013
DOI: 10.1007/s11664-013-2567-2

Dielectric and Impedance Spectroscopy of Barium Orthoniobate Ceramic

BISWAJIT PATI,[1] R.N.P. CHOUDHARY,[1,2] PIYUSH R. DAS,[1] B.N. PARIDA,[1] and R. PADHEE[1]

1.—Department of Physics, Institute of Technical Education and Research, SOA University, Bhubaneswar, India. 2.—e-mail: crnpfl@gmail.com

Barium orthoniobate ($Ba_3Nb_2O_8$), a derivative of the perovskite family, was prepared using a high-temperature solid-state reaction technique (calcination temperature = 1425°C and sintering temperature = 1450°C for 4 h). Preliminary x-ray structural analysis with room-temperature x-ray diffraction data confirmed the formation of a single-phase compound with hexagonal crystal structure. Study of the microstructure of a gold-coated pellet by scanning electron microscopy (SEM) showed that the sample has well-defined grains that are distributed uniformly throughout the surface of the sample. Detailed studies showed that the dielectric parameters (ε_r and tan δ) of the compound at three different frequencies (10 kHz, 100 kHz, and 1000 kHz) are almost constant in the low-temperature region (from room temperature to about 200°C). An anomaly in the relative permittivity (ε_r) (~357°C) suggests the possible existence of a ferroelectric–paraelectric phase transition of diffuse type in the material. Detailed studies of impedance and related parameters show that the electrical properties of the material are strongly dependent on temperature, showing good correlation with its microstructure. The bulk resistance (evaluated from impedance studies) is found to decrease with increasing temperature. This shows that the material has negative temperature coefficient of resistance (NTCR), similar to that of semiconductors. Studies of electric modulus indicate the presence of a hopping conduction mechanism in the system with nonexponential-type conductivity relaxation. The nature of the variation of the direct-current (dc) conductivity with temperature confirms the Arrhenius and NTCR behavior in the material. The alternating-current (ac) conductivity spectra show a typical signature of an ionic conducting system and are found to obey Jonscher's universal power law.

Key words: Electroceramics, impedance analysis, bulk resistance, electric modulus analysis

INTRODUCTION

Since the discovery of ferroelectricity in Rochelle salt in 1921,[1] a large number of dielectric materials of different structural families have been studied for possible industrial applications. Out of the large number of ferroelectric compounds available today, barium titanate ($BaTiO_3$) of the perovskite family of ABO_3 type (A = mono-divalent, B = tri-hexavalent ions) has attracted much attention from researchers because of its unusual properties that are useful for devices. Some of the simple or complex oxides derived from the perovskite structure are structurally more stable at room temperature.[2,3] In the process of searching for new oxides (containing rare-earth ions), the calcium oxa-metallate family has been extensively studied.[4] Such orthometallates of alkaline-earth metals, with general formula $A_3B_2O_8$ or $A_3(BO_4)_2$ (A = divalent metal, B = pentavalent metal), e.g.,

(Received January 20, 2013; accepted March 5, 2013; published online April 20, 2013)

$Ba_3V_2O_8$ and other modifications of such species, have attracted much attention from scientists because of their promising transport and ferroelectric properties and are used in solid-state devices including lasers, luminescent lamp coatings, flat-panel displays, microwave filters and antennas, etc.[5–11]

Recently, cation-deficient hexagonal (perovskite-based) materials have attracted much attention for use in applications of microwave technologies due to their low dielectric loss, relatively high permittivity, and small temperature coefficient of resonant frequency.[11–19] Among these hexagonal perovskites, some compounds with general formula $A_nB_{n-\delta}O_{3n-x}$ ($\delta \geq 1, x \geq 0$) have been prepared by varying the ratio of cubic (c) and hexagonal (h) stacking of (AO_3) layers with B-cation occupying octahedral cavities. When the cationic ratio of A to B is 3:2 (i.e., $n = 3, \delta = 2$), one of every three B-sites remains unoccupied and different structures can be formed depending on the composition and extent of anion deficiency;[20] For example, with $x = 0$, two polytypes can be adopted: (a) $Ba_5Nb_4O_{15}$-type ceramics, where the (AO_3) layers are hexagonal close packed and an empty octahedron is situated between face-sharing octahedra,[21] and (b) the 9R-type structure, where the stacking sequence is $(hhc)_3$ and a vacant octahedral cavity is located between corner-sharing octahedra. The ordered distribution of cation vacancies reduces the repulsion between B-site cations in face-sharing octahedra, hence stabilizing the crystal structure.[22] When $x = 1$ (e.g., $Ba_3Nb_2O_8$), the palmierite structure is derived from that of the 9R polytypes. In this case, oxygen-deficient cubic (AO_2) layers are formed, which forces a change in coordination of the B atoms from octahedral to tetrahedral. Further study of the BaO-rich part of the BaO–Nb_2O_5 binary system (i.e., $Ba_3Nb_2O_8$ and $Ba_4Nb_2O_9$) reveals that such compounds contain transition metals in oxidation states with d^0 electronic configuration. Because of their composition, they are sensitive to decomposition in ambient air. The crystal chemistry of the BaO–Nb_2O_5 binary system is typified by octahedral (NbO_6) units, except for $Ba_3Nb_2O_8$, which adopts the salt-like palmierite-type structure with isolated tetrahedral $(NbO_4)^{3-}$ oxyanions.[23] Apart from several structural studies on $Ba_3Nb_2O_8$ and other similar compounds, Vanderah et al.[23] reported the phase equilibria and crystal chemistry in the BaO–Nb_2O_5 systems and the same system modified by alumina. Further, Gonzalez et al.[24] studied the cation-deficient molybdenum-modified BaO-rich system using Raman spectroscopy. Recently, study of polymorphic phase transitions in $Ba_4Nb_2O_9$, one of the BaO–Nb_2O_5 systems, was reported by Bezjak et al.[25]

Detailed literature survey on these materials shows that, except for some work on structural properties and subsolidus phase equilibria of $Ba_3Nb_2O_8$ and other similar BaO-rich systems,[23–25] not much work on structural and electrical properties has been reported. In view of the importance of the material for possible device applications, in the present work we attempted to synthesize $Ba_3Nb_2O_8$ by a standard solid-state reaction route and study its structural and electrical properties for better understanding of the material.

EXPERIMENTAL PROCEDURES

Material Preparation

A polycrystalline sample of $Ba_3Nb_2O_8$ was prepared by a high-temperature solid-state reaction method (calcination temperature = 1425°C) using appropriate amounts (stoichiometric ratio) of high-purity [analytical reagent grade] precursors: $BaCO_3$ (99%; M/s s.d. Finar chem. Pvt. Ltd., India) and Nb_2O_5 (99.9%; M/s LOBA Chemie Pvt. Ltd., India). These ingredients were mixed first mechanically in an agate mortar and pestle for an hour followed by wet grinding (in methanol) for another hour to obtain a homogeneous mixture of the constituents. This mixture was finally calcined at 1425°C (decided on the basis of repeated firing/mixing) for 4 h in air. The formation of the desired compound was checked by preliminary x-ray structural analysis. The calcined powder of the compound was cold pressed into cylindrical pellets (10 mm diameter, 1 mm to 2 mm thickness) using polyvinyl alcohol (PVA) as binder, applying an isostatic pressure of 4×10^6 N/m^2. The pellets were then sintered using an optimized temperature (1450°C) and time (4 h) in air atmosphere. The sintered pellets were then polished by fine emery paper to make their faces smooth and parallel. To study the electrical properties of the compound, both of the flat and parallel surfaces of the pellets were electroded with air-drying conducting silver paste and then dried at 150°C for 8 h to remove moisture (if any) and then cooled to room temperature before taking electrical measurements.

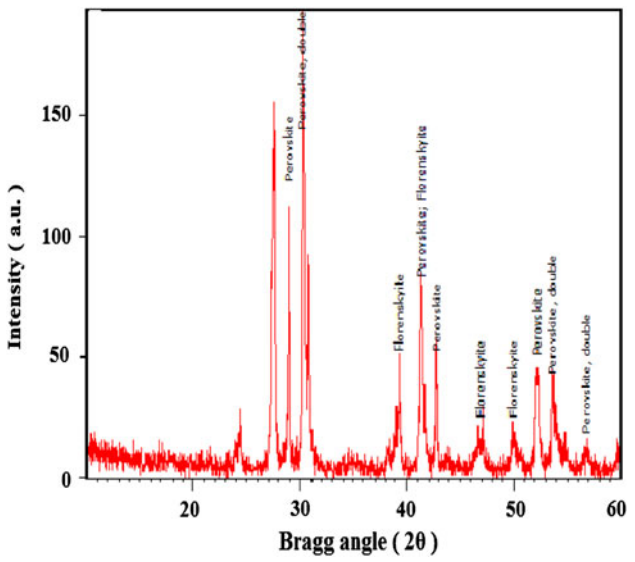

Fig. 1. XRD pattern of $Ba_3Nb_2O_8$ at room temperature.

Material Characterization

The formation and quality of the compound were checked using the x-ray diffraction (XRD) pattern of the material, recorded at room temperature using a x-ray powder diffractometer (XPERT-PRO, DISIR) with Cu K_α radiation (λ = 1.5405 Å) in a wide range of Bragg angle θ ($0° \le 2\theta \le 60°$) at scanning rate of 2°/min. The microstructure of the sintered pellet was recorded at room temperature using a scanning electron microscope (SEM, JEOL JSM-5800). The impedance and related parameters were measured as a function of temperature (30°C to 500°C) over a wide range of frequencies (100 Hz to 1 MHz) using a computer-controlled phase-sensitive meter (PSM LCR 4NL, model 1735, UK) with a laboratory-designed and fabricated sample holder and a small vertical pit furnace. A chromel–alumel thermocouple and a digital millivoltmeter (KUSAM MECO 108) were used to record temperatures. An input ac signal of small voltage amplitude (~1 V) was applied across the sample cell, followed by thermal stabilization for 2 h prior to the measurements.

RESULTS AND DISCUSSION

Structural Properties

Figure 1 shows the room-temperature XRD pattern of $Ba_3Nb_2O_8$ calcined powder. The diffraction pattern consists of a number of sharp peaks that are different from those of the ingredients. This pattern reveals better homogeneity and crystallization of the material, thus confirming the formation of a new polycrystalline single-phase compound. All the peaks of the pattern could be indexed to different crystal systems and unit cell configurations using the standard computer program package POWD. A hexagonal unit cell was selected on the basis of good agreement between observed and calculated interplanar spacing d [i.e., minimum $\sum\Delta d = \sum(d_{obs} - d_{cal})$]. The lattice parameters of the selected unit cell were refined using the least-squares subroutine of the standard computer program package.[26] These refined lattice parameters are: a = 4.4104(4) Å and c = 21.336(4) Å (the number in parenthesis being the estimated standard deviation). Using the refined lattice parameters, each peak was finally indexed and the interplanar spacing (d) of the reflection planes of the compound was calculated and compared with its observed value (Table I). The value of the coherently scattered crystallite size (average) P of the compound calculated using Scherrer equation [$P = k\lambda/(\beta_{1/2}\cos\theta)$, where k = 0.89, λ = 1.5405 Å, and $\beta_{1/2}$ is the broadening of peak at half the wavelength] was found to be 12 nm. It was found that the refined unit cell parameters with the proposed (hexagonal) crystal structure of the sample were highly consistent with those reported earlier.[23,25] As powder samples were used to obtain the XRD pattern, contributions from strain and other effects in the broadening of the XRD peaks and crystallite size calculation were ignored.

Figure 2 shows a SEM micrograph of a sintered pellet recorded at room temperature. The micrograph shows a group of small-sized grains homogeneously distributed throughout the surface of the sample. In spite of sintering at an optimized high temperature, some voids of irregular shape and dimension are still observed. Most of the grains have dimension in the range of ~2 μm to 10 μm.

Dielectric Properties

Figure 3 shows the temperature dependence of the relative permittivity (ε_r) and loss tangent (tan δ) of $Ba_3Nb_2O_8$ at some selected frequencies (10 kHz, 100 kHz, and 1 MHz). It is observed that both ε_r and tan δ decrease with increasing frequency, which is a general feature of dielectric materials.[27] The value of ε_r is almost constant in the low-temperature range (from room temperature to about 200°C), and with further increase in temperature, it increases gradually to its maximum value (ε_{max}) and then decreases. This dielectric anomaly, observed at

Table I. Comparison of d_{obs}, d_{cal}, and h k l value of all the reflections of XRD peaks

		d-Spacing			Miller Indices		
Sl. No.	**2θ (°)**	**d_{obs}**	**d_{cal}**	**Rel. Int. (I/I_0)**	**h**	**k**	**l**
1	24.36	3.6508	3.6555	10	4	2	0
2	27.61	3.2280	3.2239	88	6	0	0
3	28.86	3.0909	3.0974	63	5	2	1
4	30.26	2.9510	2.9498	100	6	1	0
5	30.85	2.8959	2.9083	44	5	0	2
6	39.25	2.2933	2.2918	23	6	2	1
7	41.40	2.1791	2.1763	41	7	3	1
8	42.76	2.1129	2.1113	22	2	1	2
9	46.91	1.9352	1.9343	08	10	0	0
10	49.86	1.8274	1.8278	7.5	8	4	0
11	52.21	1.7505	1.7496	21	9	2	1
12	53.62	1.7077	1.7082	17	7	5	1

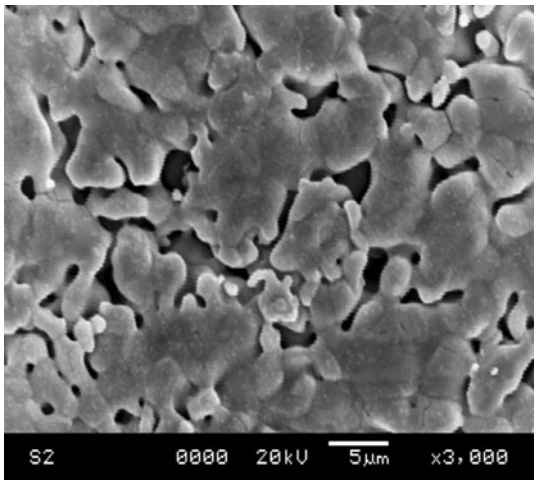

Fig. 2. SEM micrograph of $Ba_3Nb_2O_8$ at room temperature.

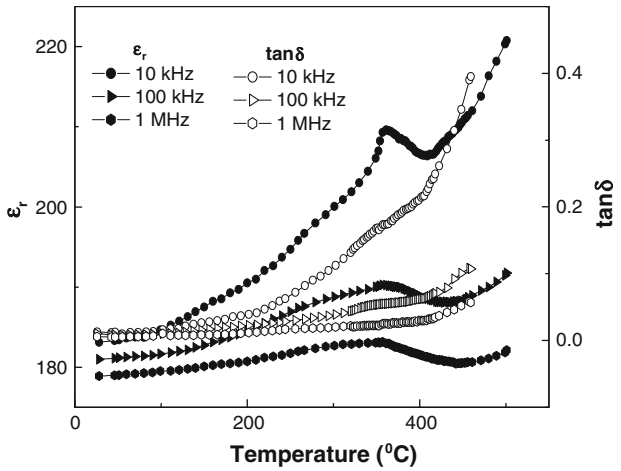

Fig. 3. Variation of ε_r and tan δ of $Ba_3Nb_2O_8$ with temperature at various frequencies.

357°C, usually referred to as the transition temperature (T_c), suggests a transition from a ferroelectric to paraelectric phase.[28] Above T_c, the increase of ε_r (at lower frequencies) may be due to space-charge polarization which arises from mobility of ions and imperfections in the material. These combined effects produce a sharp increase in the relative permittivity with increasing temperature. The maximum value of the relative permittivity at T_c (i.e., ε_{max}) for the frequencies of 10 kHz, 100 kHz, and 1 MHz are 210, 190, and 183, respectively. As the compound exhibits a frequency-independent transition temperature (i.e., no dispersion), the material is of nonrelaxor type. The relative permittivity decreases with rise in frequency because of the absence of dipolar and ionic polarization at higher frequencies.

Figure 3 further shows that the value of tan δ increases with rise in temperature. The rate of increase of tan δ in the material in the low-temperature region is slow, whereas at higher temperatures the increase is relatively sharper. This sharp increase in tan δ at higher temperatures may be due to (i) scattering of thermally activated charge carriers, (ii) some inherent defects in the sample, and (iii) creation of oxygen vacancies during sample preparation. At higher temperatures the conductivity begins to dominate, which in turn is responsible for the rise in tan δ. Again, the dispersion in tan δ at higher temperatures, an important characteristic of normal ferroelectric materials, may be attributed to nonnegligible ionic conductivity in the material arising due to loss of oxygen during sintering at high temperatures. At the same time, the defect structure along with the presence of Nb^{5+} ions accounts for its high-temperature ferroelectric behavior.[23]

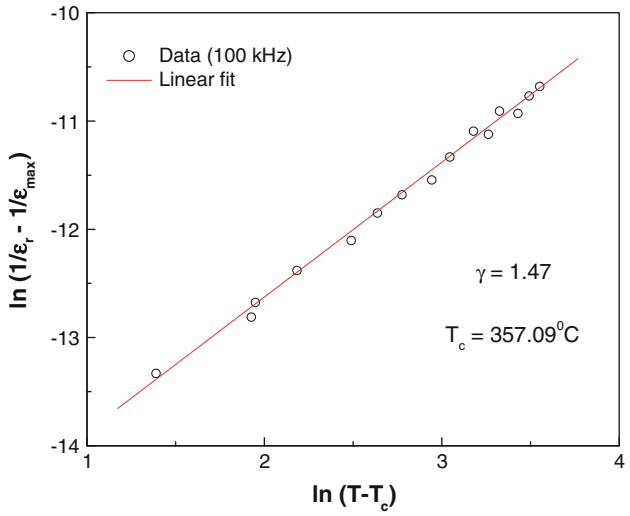

Fig. 4. $\text{Log}_e(1/\varepsilon_r - 1/\varepsilon_{max})$ versus $\text{Log}_e(T - T_c)$ plot of $Ba_3Nb_2O_8$.

The permittivity peaks are found to become broadened or diffuse with increasing frequency. To estimate the degree of diffuseness, a general expression: $\ln\left(\frac{1}{\varepsilon_r} - \frac{1}{\varepsilon_{max}}\right) = \gamma \ln(T - T_c) + \text{const.}$[29] was used, where the symbols have their usual meanings. The value of diffusivity (γ), calculated from the slope of $\ln\left(\frac{1}{\varepsilon_r} - \frac{1}{\varepsilon_{max}}\right)$ versus $\ln(T - T_c)$ plots (Fig. 4), was found to be 1.47 at 100 kHz. This value of γ ($1 < \gamma < 2$) confirms the presence of a diffuse phase transition in the material. Diffuse phase transitions are usually observed in complex and disordered systems (such as the studied compound), which can be explained by the presence of certain inequivalent positions in the elementary cell.[30]

Impedance and Modulus Spectroscopy

Complex impedance spectroscopy (CIS) is a simple nondestructive technique to study the contribution of grains, grain boundary effects, and other electrical processes in a material. The CIS technique is based on analyzing the ac response of a

system to a sinusoidal perturbation, with subsequent calculation of impedance and related parameters as a function of frequency at different temperatures.[31–33] This technique is particularly useful to separate the contributions of (i) bulk, (ii) grain boundary, and (iii) electrode polarization in the complex impedance and other related parameters along with their equivalent circuits. The impedance and related parameters of a material give data having both real (resistive) and imaginary (reactive) components. The following basic equations in terms of impedance and electrical modulus were used to study the electrical properties of the samples:

(i) Complex impedance $Z^*(\omega) = Z' - jZ'' = R_s - j/\omega C_s$
(ii) Complex electrical modulus $M^*(\omega) = \frac{1}{\varepsilon^*(\omega)} = M' + jM'' = j\omega C_0 Z^*$
(iii) Complex admittance $Y^* = Y' + jY'' = j\omega C_0 \varepsilon^* = (R_p)^{-1} + j\omega C_p$
(iv) Complex permittivity $\varepsilon^* = \varepsilon' - j\varepsilon''$
(v) Loss tangent $\tan\delta = \frac{\varepsilon''}{\varepsilon'} = -\frac{Z'}{Z''} = \frac{M''}{M'}$,

where $\omega = 2\pi f$ is the angular frequency, C_0 is the geometrical capacitance, and $j^2 = -1$. Subscripts "p" and "s" indicate the equivalent parallel and series circuit components, respectively.

The peak of the high-frequency semicircular arc in the complex impedance spectra enables us to evaluate the relaxation frequency (ω_{max} or f_{max}) of the bulk material using the relation: $\omega_{max}\tau = \omega_{max}R_bC_b = 1$ or, $1/2\pi f_{max} = R_bC_b$, where R_b and C_b are the bulk resistance and bulk capacitance, respectively.

Complex Impedance Analysis

Figure 5a, b shows complex impedance spectra (Nyquist plot) of the compound obtained at different temperatures (>250°C) over a wide range of frequency (100 Hz to 1 MHz). The impedance property of the material is characterized by the formation of semicircular arcs whose pattern of evolution changes with change in temperature. The extent of the intercept of the semicircles with the real axis (x-axis) and their number in the spectrum provide information on the kind of electrical processes occurring within the material. The correlation between these arcs and the microstructure of the material can be established using an equivalent electrical circuit. The semicircular arcs of the impedance pattern can mainly be attributed to a parallel combination of resistance and capacitance. As the temperature increases from room temperature, the straight lines progressively convert into semicircular arcs with a shift of the center towards the origin of the complex plane plot. On further increase in temperature, the slope of the line decreases and bends towards the Z'-axis (above 450°C), thus a semicircle could be observed, indicating an increase in the conductivity of the sample.[34,35] The presence of semicircular arcs for temperatures above 450°C suggests that the electrical processes in the material arise basically due to the contribution from bulk material (grain interior), which thus can be modeled as an equivalent electrical circuit (Fig. 5) comprising a parallel combination of the bulk resistance (R_b) and bulk capacitance (C_b).[36] The electrical process at high temperatures may be considered as due to intragrain phenomena. Figure 5b compares the complex impedance plots with fitted data using commercially available software (ZSIMP WIN version 2). For an ideal Debye-like response, the equivalent circuit consists of a CQR parallel combination, where Q is known as a constant-phase element (CPE). The admittance of Q is defined as $Y(\mathrm{CPE}) = A_0(j\omega)^n = A\omega^n + jB\omega^n$, with $A = A_0\cos(n\pi/2)$ and $B = A_0\sin(n\pi/2)$, where A_0 and n are frequency-independent but temperature-dependent parameters. The magnitude of the dispersion is determined by knowing the value of A_0. The value of n is such that $0 \le n \le 1$, where $n = 1$ corresponds to the behavior of an ideal capacitor and $n = 0$ represents

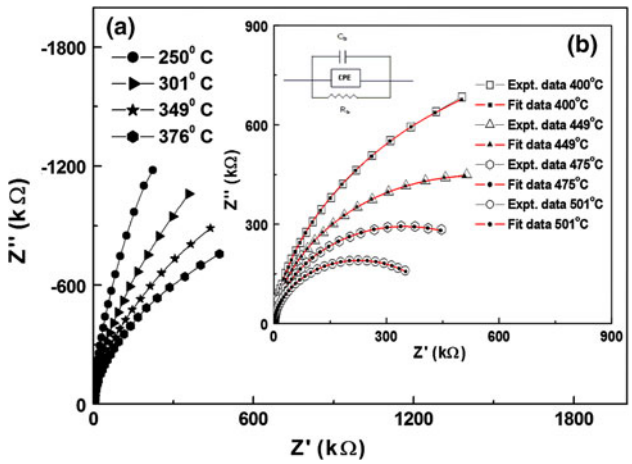

Fig. 5. Variation of Z' with Z'' of $Ba_3Nb_2O_8$ at different temperatures along with the equivalent circuit.

Table II. Bulk resistance and capacitance at different temperatures

Temperature (°C)	R_b (Ω)	C_b (F)
175	7.97×10^7	1.003×10^{-10}
200	2.519×10^7	9.645×10^{-11}
225	2.004×10^7	1.005×10^{-10}
250	1.395×10^7	1.014×10^{-10}
276	9.823×10^6	1.023×10^{-10}
301	7.465×10^6	1.029×10^{-10}
325	5.915×10^6	1.026×10^{-10}
349	4.642×10^6	1.026×10^{-10}
376	2.698×10^6	1.007×10^{-10}
400	2.148×10^6	9.998×10^{-11}
425	1.736×10^6	1.004×10^{-10}
449	1.167×10^6	9.879×10^{-10}

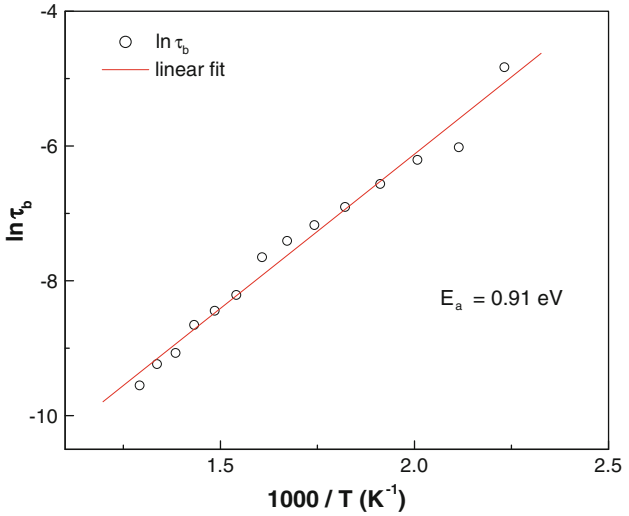

Fig. 6. Variation of relaxation time with inverse absolute temperature.

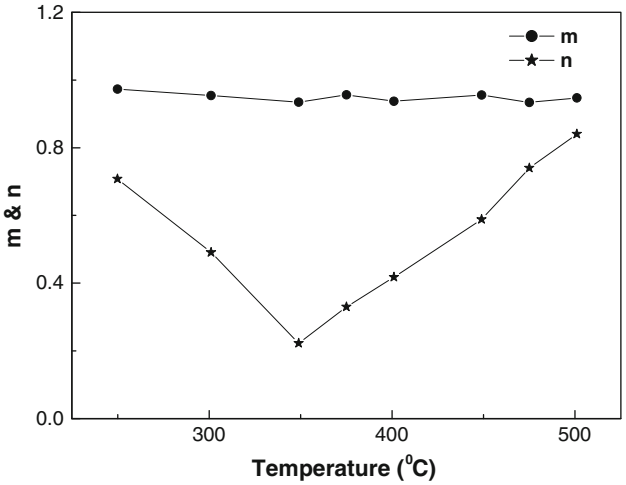

Fig. 8. Variation of the fitting parameters *m* and *n* with temperature for $Ba_3Nb_2O_8$.

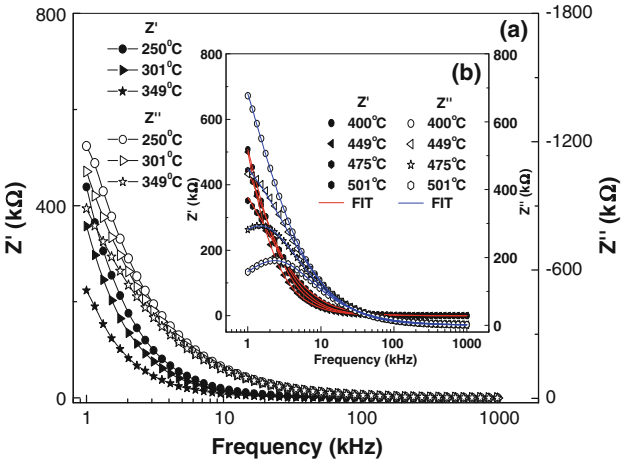

Fig. 7. Variation of Z' and Z'' of $Ba_3Nb_2O_8$ with frequency at different temperatures.

that of an ideal resistor.[37,38] From fitting the curves, the calculated values of bulk resistance (R_b) and bulk capacitance (C_b) at different temperatures are compared in Table II. The decrease in R_b with the rise in temperature suggests NTCR behavior of the compound.[39] This NTCR characteristic is also observed in the frequency-dependent Z' plot.

For ideal Debye-type relaxation, a perfect semicircle with center on the Z'-axis should be observed. However, in the studied material, depressed semicircles corresponding to non-Debye-type relaxation are observed. It is also seen that there is a distribution of relaxation time instead of a single relaxation time in the material.[39,40] The intercept of each semicircle with the real Z'-axis gives the value of the bulk and grain boundary contributions to the resistance/impedance. The semicircles in the impedance spectrum have a characteristic peak occurring at a unique relaxation frequency, usually referred to as the resonance frequency (f_r) ($\omega_r = 2\pi f_r$). It can be expressed as $\omega_r RC = \omega_r \tau = 1$, and thus $f_r = 1/2\pi RC$, where τ is the relaxation time. The relaxation time due to bulk effect (τ_b) has been calculated using the equation $\omega_r \tau_b = 1$, or $\tau_b = 1/2\pi f_r$.

Figure 6 shows the variation of ln τ_b with inverse absolute temperature (1000/T). The value of τ_b decreases with rise in temperature, and thus the temperature-dependent relaxation time for bulk material follows the Arrhenius relation: $\tau = \tau_0 \exp(-E_a/K_B T)$, where τ_0 is the pre-exponential factor, K_B is the Boltzmann constant, and T is the absolute temperature. Careful comparison of the temperature-dependent bulk relaxation time with that of the proposed model shows very good agreement, indicating the validity of the model and accuracy of the experimental data. The calculated value of activation energy (E_a) was found to be 0.91 eV.

Figure 7a and b show the variation of the real and imaginary parts of the impedance (Z' and Z'') with frequency at different temperatures. The values of Z' decrease with rise in frequency and temperature, which is related to the electrical conductivity of the material.[27] In the low-frequency region, there is a decrease in the magnitude of Z' with rise in temperature, indicating negative temperature coefficient of resistance (NTCR) behavior. This behavior changes drastically in the high-frequency region, showing complete merger of the Z' plots above a certain fixed frequency. At high frequency, the Z' values at each temperature coincide, implying a possible release of space charge.[11] The reduction in the barrier properties of the materials with rise in temperature may be a factor responsible for the enhancement of the ac conductivity of the materials at higher frequencies.[34,35] The particular frequency at which Z' becomes independent of frequency was observed to shift towards the higher-frequency side with rise in temperature. This shift in the Z' plateau indicates

the existence of a frequency relaxation process in the material. The curves display a single relaxation process and indicate an increase in ac conductivity with increase in temperature and frequency.[41]

The loss spectrum of the material can be characterized by a few important features, such as: (i) a monotonic decrease in Z'' in the low-temperature region, (ii) the appearance of peaks in the loss spectrum at high temperatures, (iii) a significant increase in peak broadening with increase in temperature, and (iv) the existence of symmetric peak broadening. The absence of peaks up to a temperature of 449°C in the loss spectrum suggests the absence of current dissipation in this temperature region. The pattern shows peaks at a particular frequency which describes the type and strength of the electrical relaxation phenomenon in the materials.[41] The value of Z'' reaches a maximum peak (Z''_{max}) above 450°C. It is expected that low-temperature (<450°C) peaks were beyond the range of the frequencies applied. Z''_{max} shifts to the higher-frequency side with increasing temperature, indicating an increase of the tangent loss in the samples. The significant increase in the broadening of the peaks with increase in temperature suggests the existence of a temperature dependence of the electrical relaxation phenomenon in the materials. The relaxation process may be due to the presence of electrons/immobile species at low temperatures and defects/vacancies at higher temperatures.[37,42] The asymmetric broadening of the peaks suggests a spread of relaxation time with two equilibrium positions. The peak heights are proportional to the bulk resistance (R_b) and can be estimated and explained by the equation $Z'' = R_b[\omega\tau/(1 + \omega^2\tau^2)]$ in the Z'' versus frequency plots. Further, the magnitude of Z'' decreases gradually with a shift in the peak frequency towards the high-frequency side, finally merging in the high-frequency region. This is an indication of accumulation of space charge in the material.[28]

Again, the imaginary part of the impedance plot indicates that the high-frequency slopes are independent of temperature. On the other hand, the low-frequency slopes are strongly temperature dependent. These two types of temperature dependence of the slopes suggest that there are two distinct dispersion mechanisms involved in the sample. The asymmetric behavior, which is similar to other ferroelectrics,[43,44] can be explained using the CQR equivalent circuit as shown in Fig. 5b, where $C = A(j\omega)^{m-1}$ and $Q = A(j\omega)^{n-1}$ are Jonscher's universal capacitances.[45] The frequency dependence of the ac complex impedance can be expressed as $Z^* = R_0/[1 + (j\omega/\omega_1)^m + (j\omega/\omega_2)^n]$,[44] where $\omega_1 = 2\pi f_1$ and $\omega_2 = 2\pi f_2$ are the first and second characteristic angular frequencies, respectively, and the exponents m and n correspond to the slopes at high and low frequencies, respectively. Excellent agreement between the experimental and calculated values for both the real and imaginary parts of impedance is observed from nonlinear curve fitting (Fig. 7) using the formula $Z'' = R_0/[(\omega/\omega_1)^m + (\omega/\omega_2)^{-n}]$.[44]

The variation of the fitting parameters (m and n) with temperature (calculated from Z'' versus frequency) is shown in Fig. 8. It is seen that m is close to unity and temperature independent. On the other hand, the value of n is much less than one, and it is temperature dependent. In the ferroelectric phase, the value of n decreases and becomes minimum at T_c, subsequently increasing with temperature. The minimum value of n at T_c can be explained by the restoring force between charge carriers and the lattice.[44] The above variation in the value of n can also be understood based on the theory proposed by Dissado and Hill.[46,47] According to them, the exponent n characterizes the magnitude of the correlation in a single dipole reorientation. A unity value corresponds to fully correlated transitions, and a zero value corresponds to fully uncorrelated transitions. In the present work, n tends to a minimum around T_c, suggesting strongly uncorrelated reorientation of the charge carrier polarization at the transition point.

Complex Electric Modulus Analysis

The complex electric modulus formalism is widely used for differential study of electrode polarization effects and grain boundary conduction processes. It is also useful to detect bulk properties, electrical conductivity, and relaxation time.[36,37,48] Therefore, this technique provides insight into the electrical processes occurring in a material at different temperatures and frequencies. The following relations are normally used to estimate M' and M'':

$$M' = B\left[\frac{(\omega RC)^2}{1+(\omega RC)^2}\right] = B\left[\frac{\omega^2\tau^2}{1+\omega^2\tau^2}\right],$$

$$M'' = B\left[\frac{\omega RC}{1+(\omega RC)^2}\right] = B\left[\frac{\omega\tau}{1+\omega^2\tau^2}\right],$$

$$\text{where } B = \frac{C_0}{C}.$$

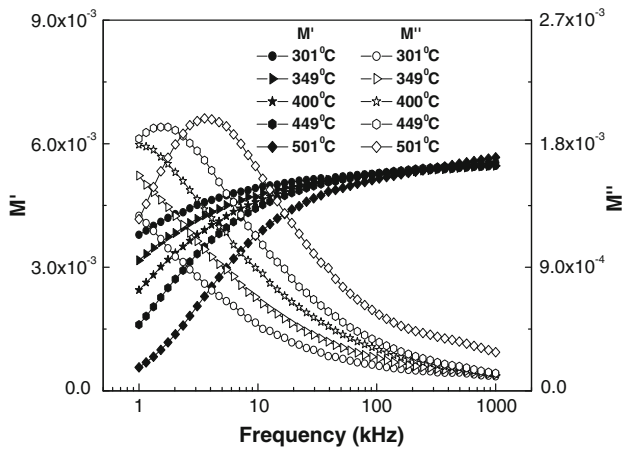

Fig. 9. Variation of M' and M'' with frequency at different temperatures for $Ba_3Nb_2O_8$.

This also enables the determination of the inhomogeneous nature of polycrystalline samples due to the effect of bulk and grain boundary, which cannot be distinguished in complex impedance plots. The other major advantage of the electric modulus formalism is suppression of the electrode effect.

Figure 9 shows the variation of M' and M'' with frequency at selected temperatures (>300°C). The value of M' approaches zero on lowering the frequency with monotonic dispersion, whereas with rise in frequency the values of M' coincide. This may be due to the presence of a conduction phenomenon and short-range mobility of charge carriers. This implies that there is a lack of a restoring force for flow of charges under the influence of a steady electric field.[36] The plot reveals that the M''_{max} peak shifts to the higher-frequency side. This feature of the dielectric relaxation suggests that a hopping mechanism of charge carriers dominates intrinsically at higher temperatures in a thermally activated process. The asymmetric broadening of the peak indicates a spread of relaxation with different time constants, which in turn suggests that the relaxation in the material is of non-Debye type.[48]

The imaginary components of the impedance (Z'') and modulus (M'') are plotted at some selected higher temperatures in Fig. 10. Such combined plots of Z'' and M'' as a function of frequency are normally used to detect the presence of the smallest capacitance and the largest resistance, as suggested by Sinclair et al.[49] This helps in distinguishing between relaxation processes due to short- versus long-range movement of charge carriers. If the process is short range, both peaks (Z'' versus frequency and M'' versus frequency) will occur at different frequencies, whereas for long-range movement of charge carriers both peaks will occur at the same frequency.[49,50] Figure 10 shows an appreciable mismatch between the peaks of Z'' and M'' at selected temperatures. This result suggests (i) the presence of localized movement of charge carriers, (ii) departure from ideal Debye-like behavior, and (iii) a distribution of relaxation times in the material.[51,52]

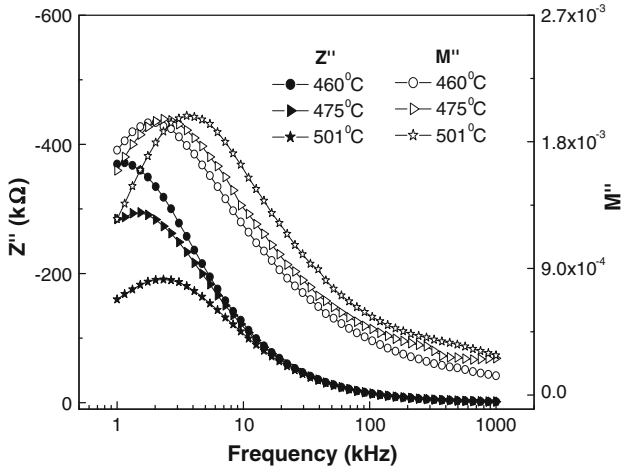

Fig. 10. Variation of Z' and M' with frequency at different temperatures for $Ba_3Nb_2O_8$.

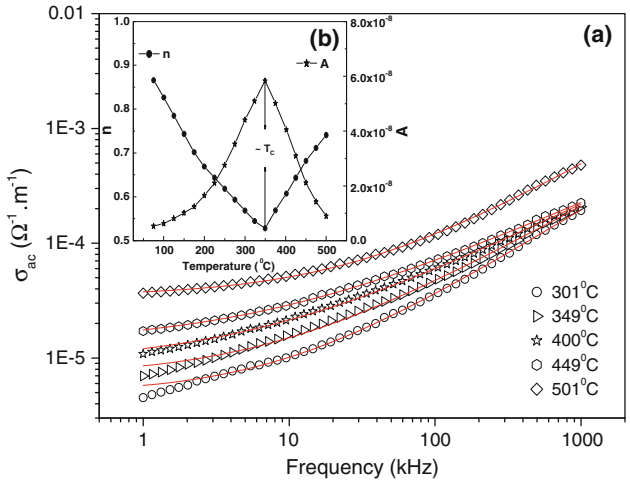

Fig. 11. (a) Variation of σ_{ac} of $Ba_3Nb_2O_8$ as a function of frequency at various temperatures. (b) Variation of ac fitting data A and n with temperature.

AC Conductivity Analysis

The phenomenon of conductivity dispersion in solids is generally analyzed using Jonscher's power law: $\sigma_{ac} = \sigma_{dc} + A\omega^n$, where σ_{dc} is the dc conductivity at a particular temperature, A is a temperature-dependent constant, and n is a temperature-dependent exponent in the range $0 < n < 1$. Here, n represents the degree of interaction between mobile ions and the lattice around them, and A determines the strength of polarizability.[53]

The frequency dependence of the ac conductivity [$\sigma_{ac}(\omega)$] at various temperatures is shown in Fig. 11a. In the low-temperature region, the conductivity increases with increase in frequency, which is a characteristic of ω^n. At higher temperatures and low frequencies, the conductivity shows a flat response, while it has ω^n dependence at high frequencies. The conductivity curves show dispersion in the low-frequency region. From the graphs it is clear that σ_{ac} increases with rise in frequency, but it is nearly independent at low frequency. Extrapolation of this part towards the lower-frequency side gives the value of σ_{dc}. The increasing trend of σ_{ac} with rise in frequency in the lower-frequency region may be attributed to the disordering of cations between neighboring sites and the presence of space charge.[54] In the high-frequency region the curves approach each other.

According to Jonscher,[37] the origin of the frequency dependence of conductivity lies in the relaxation phenomena arising due to mobile charge

carriers. When a mobile charge carrier hops to a new site from its original site, it remains in a state of displacement between two potential energy minima. Also, the conduction behavior of the materials obeys the power law $\sigma(\omega) \propto \omega^n$ with a change of slope governed by n in the low-temperature region. A value of n less than 1 signifies that the hopping process involves translational motion with sudden hopping of charge carriers, whereas $n > 1$ means that the motion involves localized hopping without the species leaving the neighborhood.[11,38] The frequency at which the change in slope takes place is known as the hopping frequency of polarons (ω_p) and is temperature dependent. The high-frequency dispersion has been attributed to the ac conductivity, whereas the frequency-independent plateau region corresponds to the dc conductivity. The material obeys the universal power law, as confirmed by fitting of the above equation to the experimental data, as also shown in Fig. 11a. From nonlinear fitting it is found that the motion of the charge carriers is translational, because of the small value of n (<1).[55] The dc conductivity increases with rise in temperature (as expected) in the given material.

Figure 11b shows the variation of A and n with temperature. It is seen that the value of n decreases with rise in temperature and becomes minimum near the transition temperature T_c of the material. Again it increases with increase in temperature, whereas the pre-exponential factor A shows the opposite trend. The exponent n represents the interaction between the mobile ions and the lattice around them.[53] The observed minimum at T_c suggests strong interaction between the lattice and mobile ions. According to dynamic theory,[44,45] one of the transverse optical modes (soft mode) is weakened, and the restoring force tends to zero at T_c. Therefore, the charge carriers coupled with the soft mode become highly mobile at T_c, and thus the conductivity will increase. The pre-exponential factor A determines the strength of polarizability. The maximum value of A at T_c suggests high polarizability (i.e., maximum permittivity) of the material.[53]

DC Conductivity Analysis

The dc electrical conductivity of the (bulk) material is obtained using $\sigma_{dc} = t/R_bA = t(\text{slope})/A$, where t and A represent the thickness and area of the sample, respectively. Figure 12a shows the temperature dependence of the dc conductivity of the material. It is observed that σ_{dc} increases with rise in temperature, which further supports the NTCR behavior of the sample. The nature of the plot follows the Arrhenius relation $\sigma_{dc} = \sigma_0 \exp(E_a/K_BT)$.[48] The occurrence of different slopes at different temperature regions suggests the presence of multiple conduction processes in the sample with different activation energies.[55,56] The activation energy (E_a) of the sample, calculated in the low- (225°C to 325°C) and high-temperature ranges (425°C to 501°C), are 0.32 eV and 0.49 eV, respectively. It is found that these values of E_a are different from the values calculated from the relaxation time plots. This implies that the charge carriers that are responsible for conduction and relaxation processes are different. Also, the difference in the value of activation energy in the low- and high-temperature ranges supports the hopping-type conduction mechanism in the material.[53] Figure 12b shows the temperature dependence of the dc conductivity found from the ac conductivity fitting. The nature of the plot and the activation energy is consistent and also are in good agreement with that obtained directly. The small value of E_a suggests that the material can be activated by applying a relatively small energy.

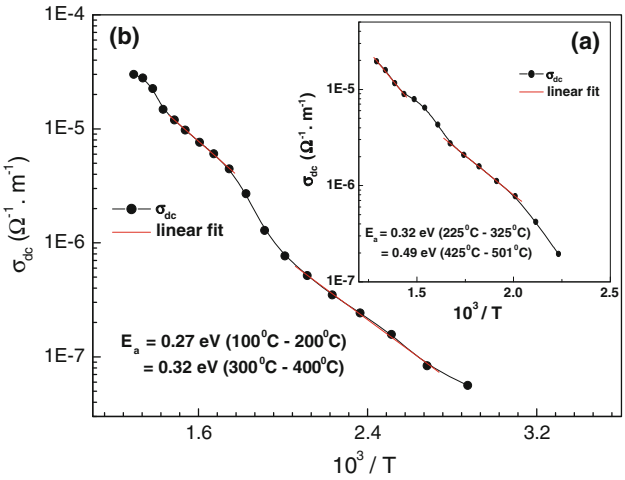

Fig. 12. Variation of σ_{dc} of $Ba_3Nb_2O_8$ with inverse absolute temperature.

CONCLUSIONS

A polycrystalline sample of $Ba_3Nb_2O_8$ was prepared by a high-temperature solid-state reaction technique. Preliminary x-ray analysis shows a hexagonal crystal structure of the compound at room temperature. The surface morphology of the compound, studied by SEM, shows homogeneously distributed grains. The dielectric study reveals that the material has relatively high permittivity and undergoes a transition from a ferroelectric to paraelectric phase at 357°C. The compound shows low loss even at 500°C (0.39 at 10 kHz), which decreases with increasing frequency (i.e., 0.11 at 100 kHz and 0.06 at 1 MHz). Due to low loss, the quality factor of the material is high. Characteristics such as the relatively high permittivity, low dielectric loss, and high quality factor make this material a potential candidate for many applications, including microwave dielectric resonators. The complex impedance plots reveal that the material exhibits (i) electrical transport (conduction) due to bulk material, (ii) negative temperature coefficient of resistance (NTCR)-type

behavior, and (iii) a temperature-dependent relaxation phenomenon. Complex impedance analysis suggests that the dielectric relaxation in the material is of polydispersive non-Debye type. The impedance spectrum has been used to estimate the electrical conductivity. The complex electrical modulus analysis indicated nonexponential type of conductivity relaxation in the material. The minimum value of the impedance fitting parameter (n) around the transition temperature supports the existence of ferroelectric properties in the material. The activation energy of the sample as estimated from the conductivity pattern and relaxation time pattern are different. This suggests that the charge carriers that are responsible for conduction and relaxation processes are different. The frequency dependence of the ac conductivity obeys Jonscher's universal power law.

ACKNOWLEDGEMENTS

The authors would like to acknowledge the kind help of Dr. B. Mishra, principal scientist, Dalmia Institute of Scientific and Industrial Research (DISIR), Rajgangpur, Odisha and IIT Kharagpur for carrying out some experimentation.

REFERENCES

1. J. Valsek, *Phys. Rev.* 17, 475 (1921).
2. K. Uchino, *Ferroelectric Devices* (New York: Marcel Dekker, 2000).
3. M.E. Lines and A.M. Glass, *Principle and Application of Ferroelectrics and Related Materials* (Oxford: Clarndon, 1977).
4. L.H. Brixner, P.L. Flournoy, and J. Elect, *Chem. Soc.* 112, 303 (1965).
5. A. Grzechnik and P.F. McMillan, *Solid State Commun.* 102, 569 (1997).
6. L.D. Merkle, A. Pinto, H. Verdun, and B. McIntosh, *Appl. Phys. Lett.* 61, 2386 (1992).
7. B. Buijsse, J. Schmidt, I.Y. Chan, and D.J. Singel, *Phys. Rev. B* 51, 6215 (1995).
8. P. Parhi, V. Manivanan, S. Kohli, and P. McCurdy, *Bull. Mater. Sci.* 31, 885 (2008).
9. A.M. Glass, S.C. Abrahams, A.A. Ballmann, and G. Laiacono, *Ferroelectrics* 17, 579 (1978).
10. R. Umemura, H. Ogawa, A. Yokoi, H. Ohsato, and A. Kan, *J. Alloy. Compd.* 424, 388 (2006).
11. B. Pati, B.C. Sutar, P.R. Das, and R.N.P. Choudhary, *J. Mater. Sci: Mater. Electron.* (2012). doi:10.1007/s10854-012-0983-3.
12. H. Sreemoolanadhan, M.T. Sebastian, and P. Mohanan, *Mater. Res. Bull.* 30, 653 (1995).
13. C. Vineis, P.K. Davies, T. Negas, and S. Bell, *Mater. Res. Bull.* 31, 431 (1996).
14. S. Kamba, J. Petzelt, E. Buixaderas, D. Haubrich, P. Vanek, P. Kuzel, I.N. Jawahar, M.T. Sebastian, and P. Mohanan, *J. Appl. Phys.* 89, 3900 (2001).
15. S.M. Moussa, J. Claridge, M.J. Rosseinsky, S. Clark, R.M. Ibberson, T. Price, D.M. Idles, and D.C. Sinclair, *Appl. Phys. Lett.* 82, 4537 (2003).
16. F. Zhao, Z. Yue, J. Pei, H. Zhuang, Z. Gui, and L. Li, *Appl. Phys. Lett.* 89, 202901 (2006).
17. P. Mallinson, J.B. Claridge, D.M. Idles, T. Price, R.M. Ibberson, M. Allix, and M.J. Rosseinsky, *Chem. Mater.* 18, 6227 (2006).
18. F. Zhao, H. Zhuang, Z. Yue, J. Pei, Z. Gui, and L. Li, *Mater. Lett.* 61, 3466 (2007).
19. F. Zhao, Z. Yue, J. Pei, Z. Gui, and L. Li, *Appl. Phys. Lett.* 90, 142908 (2007).
20. E.G. Gonzalez, M. Parras, and J.M.G. Calbet, *Chem. Mater.* 10, 1576 (1998).
21. B. Mossner and S.K. Sack, *J. Less-Common Met.* 114, 333 (1985).
22. G. Trolliard, N. Teneze, P. Boullay, and D. Mercurio, *J. Solid State Chem.* 177, 1188 (2004).
23. T.A. Vanderah, T.R. Collins, W. Wong-Ng, R.S. Roth, and L. Farber, *J. Alloy. Compd.* 346, 116 (2002).
24. E.G. Gonzalez, M. Parras, and J.M.G. Calbet, *Chem. Mater.* 12, 2287 (2000).
25. J. Bezjak, A. Recnik, B. Jancar, P. Boullay, I.R. Evans, and D. Suvorov, *J. Am. Ceram. Soc.* 55, 492 (1972).
26. E. Wu, POWD, an interactive powder diffraction data interpretation and indexing program, Ver. 2.1, School of Physical Sciences, Flinders University South Bedford Park, SA 5042 Australia.
27. J.C. Anderson, *Dielectrics* (London: Chapman & Hall).
28. P.R. Das, B. Pati, B.C. Sutar, and R.N.P. Choudhary, *Adv. Mater. Lett.* 3, 8 (2012).
29. S.M. Pilgrim, A.E. Sutherland, and S.R. Winzer, *J. Am. Ceram. Soc.* 73, 3122 (1990).
30. L.E. Cross, *Ferroelectrics* 76, 241 (1987).
31. S. Sen and R.N.P. Choudhary, *Mater. Chem. Phys.* 87, 256 (2004).
32. S. Brahma, R.N.P. Choudhary, and A.K. Thakur, *Phys. B* 355, 188 (2005).
33. J.R. Macdonald, *Impedance Spectroscopy Emphasizing Solid Materials and Systems (Chapter 4)* (New York: Wiley, 1987).
34. V. Provenzano, L.P. Boesch, V. Volterra, C.T. Moynihan, and P.B. Macedo, *J. Am. Ceram. Soc.* 55, 492 (1972).
35. H. Jain, C.H. Hsieh, and J. Non-Cryst, *Solids* 172, 1408 (1994).
36. I.M. Hodge, M.D. Ingram, and A.R. West, *J. Electroanal. Chem.* 58, 429 (1975).
37. A.K. Jonscher, *Nature* 267, 673 (1977).
38. R. Padhee, P.R. Das, B.N. Parida, and R.N.P. Choudhary, *J. Mater. Sci.: Mater. Electron.* 23, 1688 (2012).
39. S. Sen, S. Sen, R.N.P. Choudhary, and P. Pramanik, *Phys. B* 38, 756 (2007).
40. B. Behera, P. Nayak, and R.N.P. Choudhary, *J. Alloy. Compd.* 436, 226 (2007).
41. S. Chatterjee, P.K. Mahapatra, R.N.P. Choudhary, and A.K. Thakur, *Phys. Stat. Sol. (a)* 201, 588 (2004).
42. C.K. Suman, K. Prasad, and R.N.P. Choudhary, *J. Mater. Sci.* 41, 369 (2006).
43. J.S. KiM and J.N. Kim, *Jpn. J. Appl. Phys.* 39, 3502 (2000).
44. Z. Lu, J.P. Bonnet, J. Ravez, J.M. Reau, and P. Hagenmuller, *Phys. Chem. Solids* 53, 1 (1992).
45. A.K. Jonscher, *Dielectric Relaxation in Solids* (London: Chelesa Dielectric, 1983).
46. L.A. Dissado and R.H. Hill, *Nature* 279, 685 (1979).
47. L.A. Dissado and R.H. Hill, *Philos. Mag. B* 41, 625 (1980).
48. J.R. Macdonald, *Solid State Ionics* 13, 147 (1984).
49. D.C. Sinclair and A.R. West, *J. Appl. Phys.* 66, 3850 (1989).
50. M.A.L. Nobre and S. Lanfredi, *J. Appl. Phys.* 93, 5557 (2003).
51. B.N. Parida, P.R. Das, R. Padhee, and R.N.P. Choudhary, *J. Alloy. Compd.* 540, 267 (2012).
52. S. Saha and T.P. Sihna, *Phys. Rev. B*. **65**, 134103 (2002).
53. D.K. Pradhan, R.N.P Choudhary, C. Rinaldi and R.S. Katiyar, *J. Appl. Phys*. 106, 24102 (2009).
54. R.N.P. Choudhary, D.K. Pradhan, C.M. Tirado, G.E. Bonilla, and R.S. Katiyar, *J. Mater. Sci.* 42, 7423 (2007).
55. D.K. Pradhan, B. Behera, and P.R. Das, *J. Mater. Sci.: Mater. Electron.* 23, 779 (2012).
56. Z. Lu, J.P. Bonnet, J. Ravez and J.P. Hagenmuller, *Solid State Ionics* 57, 235 (1992).